AIAA JOURNAL
Vol. 30, No. 4, April 1992

Assessment of Total Variation Diminishing Schemes in Compressible Mixing Flow Computations

Pong-Jeu Lu* and Kuen-Chuan Wu†
National Cheng Kung University, Tainan, Taiwan 70101, Republic of China

Numerical simulations of temporally developing mixing layers using high-resolution total variation diminishing (TVD) schemes have been carried out to investigate the effects of grid resolution and inherent scheme dissipation on the solution quality. Owing to the sensitivity of the turbulence results to grid resolution, mixing flow computations generally require high grid density to resolve the shear-layer dynamics and to interpret the mean and turbulent flowfield interactions. Various limiters were tested in examining the numerical dissipation effect for which essentially nonoscillatory (ENO) solution is taken as a benchmark basis. The computations performed for scheme evaluation covered a broad spectrum including subsonic, transonic, and supersonic convective Mach numbers. Among the schemes considered, the performance of a minmod and van Leer limiters comply more consistently with the ENO results for a wide range of convective Mach numbers, whereas the superbee limiter, being the test TVD scheme for subsonic and low transonic Mach number flow, suffers from overcompression, which may lead to nonphysical solutions at high supersonic convective Mach numbers. The result obtained by each TVD scheme is sensitive to the design of the limiter. Dissipation introduced by the limiting procedure should be kept as minimal as possible, but a nonsmooth minimization should be avoided, because it may result in nonphysical overcompression, particularly for high convective Mach number flows.

I. Introduction

COHERENT pairing of large-scale vortical structures in incompressible turbulent mixing layers has been discovered in a variety of flows with a wide range of Reynolds numbers.[1-3] Subharmonic frequency forcings were found to be the key mechanism for this type of rapid mixing and have been utilized in many mixing flow control or enhancement applications.[4] However, as flow Mach number increases, the growth rate of the mixing layer decreases and reduces to a very low asymptotic value in the supersonic convective Mach number regime.[5,6] Because the success of the current interest in developing supersonic combustion ramjet (scramjet) engines for transatmospheric vehicles depends critically on the flow mixing condition, much effort has been focused on both elucidating the underlying instability mechanism and developing mixing enhancement techniques for the supersonic mixing layers. To date only a limited number of experiments[5-7] and analyses[8-12] have been conducted regarding the exploration of the basic flow structure responsible for this low spreading rate. Linear instability analyses have been very fruitful in providing insights about the stability characteristics of the compressible shear layer. Nevertheless, they cannot be applied to flows with large-scale vortical structures, nor can they explain flows with nonlinear (shock) waves present. As for experiments, owing to the complexity in establishing reliable measurement systems, experimental investigations[5-7] of high speed compressible mixing layers are quite few so far and most of the studies concerning basic flow structure rely mainly on flow visualizations. Numerical simulation arises as a viable complement to experiment, which is of great potential for not only providing nonintrusive and detailed flow investigation but also facilitating the identification of the important parameters involves. Therefore, the assessment of whether fundamental physics pertaining to compressible mixing flow can be predicted correctly by the numerical schemes used is of paramount importance and must be done before numerical simulation can be generally accepted as a reliable tool.

Three main categories of numerical methods, namely, spectral/pseudospectral methods, vortex methods, and finite difference and finite volume methods, have been applied to the study of the mixing flow problems. The advantages and disadvantages associated with each numerical method have been critically reviewed by Jou and Riley.[13] Spectral/pseudospectral and vortex methods all suffer from their deficiency in treating discontinuities occurring in the supersonic flowfields. Thus, most of the compressible mixing layer computations used the finite difference or finite volume method approach.[11,14-16] Recently developed total variation diminishing (TVD)-type high resolution schemes have gained popularity for their wide applications in compressible flow, in particular the shock and discontinuity capturing problems.[17-19] TVD schemes contain self-adjusted numerical dissipation, which occurs around the local extrema and discontinuity points. How these inherent dissipations affect the mixing flow simulation has not yet been fully investigated. The present work attempts to study this issue by comparing the computed TVD results using different limiters to those of the essentially nonoscillatory (ENO) scheme. Temporally growing shear-layer simulations including subsonic, transonic, and supersonic cases were performed. It was found that both grid resolution and constituent limiters of the TVD schemes may influence the accuracy of the numerical simulation, and the discrepancy in results would become progressively enlarged when convective Mach number increases.

II. Numerical Formulation

A. Governing Equations

The conservation laws for the inviscid, homogeneous mixing flow can be expressed in an integral form in Cartesian coordinates x and y as follows:

$$\frac{\partial}{\partial t}\int_v U\,dV + \oint_s \boldsymbol{n}\cdot\boldsymbol{F}\,dS = 0 \tag{1}$$

In the above equation the set of conservative variables and

Received Oct. 15, 1990; revision received June 4, 1991; accepted for publication July 17, 1991.

*Associate Professor, Institute of Aeronautics and Astronautics.
†Graduate Research Assistant, Institute of Aeronautics and Astronautics.

the normal flux vector component $F_n = \boldsymbol{n} \cdot \boldsymbol{F}$ are defined respectively by the column vectors:

$$U = \begin{pmatrix} \rho \\ \rho u \\ \rho v \\ e \end{pmatrix}, \quad F_n = \begin{pmatrix} \rho u_n \\ \rho u u_n + p n_x \\ \rho v u_n + p n_y \\ (e + p) u_n \end{pmatrix} \tag{2}$$

where ρ, p, e, u, and v stand for density, pressure, total energy and the velocity components of $\boldsymbol{u}$ in x and y directions, respectively; $u_n = \boldsymbol{u} \cdot \boldsymbol{n}$ is the normal velocity; and n_x and n_y are the projections of the unit normal $\boldsymbol{n}$ in x and y directions.

Pressure can be obtained from the equation of state:

$$p = (\gamma - 1)\left(e - \frac{\rho}{2}\boldsymbol{u} \cdot \boldsymbol{u}\right) \tag{3}$$

In the present study of temporally-growing shear layers, the reference length and time scales are chosen respectively to be half of the initial vorticity thickness of the shear layer $\delta_\omega/2$ and $\delta_\omega/2\bar{c}$, $\bar{c}$ being the sound speed of the initial mean flow; velocity components are nondimensionalized by $\bar{c}$ and density by the initial mean flow value. Thermodynamic quantities p and e are nondimensionalized by $\rho\bar{c}^2$.

B. TVD Schemes and Numerical Dissipations

A finite volume approach is adopted to discretize the integral conservation laws Eq. (1) into a semidiscretized equation:

$$\frac{\partial}{\partial t}(U_{i,j} V_{i,j}) + \sum_k \boldsymbol{n}_k \cdot \tilde{\boldsymbol{F}}_k S_k = 0 \tag{4}$$

where the sum of the flux terms refers to all the external sides of the control volume, $V_{i,j}$, and $U_{i,j}$ is the cell-averaged conservative variable. TVD schemes[20] using various flux limiters[21] are implemented for the construction of the numerical flux function $\tilde{\boldsymbol{F}}_k$. A typical second-order TVD scheme adopted herein takes the form[19]:

$$\tilde{F}_{j+1/2} = \frac{1}{2}[F_j + F_{j+1} + R_{j+1/2}\phi_{j+1/2}] \tag{5a}$$

$$\phi^\ell_{j+1/2} = \sigma(a^\ell_{j+1/2})\,(g^\ell_j + g^\ell_{j+1}) - \psi(a^\ell_{j+1/2} + \gamma^\ell_{j+1/2})\,\alpha^\ell_{j+1/2} \tag{5b}$$

$$\gamma^\ell_{j+1/2} = \sigma(a^\ell_{j+1/2}) \begin{cases} (g^\ell_{j+1} - g^\ell_j)/\alpha^\ell_{j+1/2} & \alpha^\ell_{j+1/2} \neq 0 \\ 0 & \alpha^\ell_{j+1/2} = 0 \end{cases} \tag{5c}$$

$$\sigma(z) = -\frac{1}{2}\left[\psi(z) - \frac{\Delta t}{V} z^2\right] \tag{5d}$$

where $F_j = F_n(U_j)$ is defined by Eq. (2), and $R_{j+1/2}$ is a transformation matrix constructed using the Roe's averaged[22] right eigenvectors of the Jacobian matrix $A = \partial F_n/\partial U$. Variables $\phi^\ell_{j+1/2}$ and $\alpha^\ell_{j+1/2}$ correspond to the ℓth elements of vectors $\Phi_{j+1/2}$ and $R^{-1}_{j+1/2}(U_{j+1} - U_j)$ respectively, in which R^{-1} is the left eigenvector matrix of A. Function $\psi(z)$ contains an entropy correction[20] to $|z|$ and g^ℓ_j is the limiter function to be discussed later. With the choice of Eq. (5d), scheme Eq. (5) is second-order accurate in space and time except near the discontinuity and extremal points where the modified flux is limited by the limiter function, making the scheme degenerate to locally first-order accurate.

Both Euler explicit (second order in time and space) and third-order Runge-Kutta time-stepping[23] methods have been used to integrate Eq. (4). The time step size was chosen to be $\Delta t = 0.03$ (approximately $CFL = 0.3$) in order to resolve the small-scale fluctuation field. From testing several mixing flow simulations, it was found that with such a small time step there are no appreciable differences between using these two time integration methods. Multistage Runge-Kutta stepping, in general, consumes much more computational time than does the Euler explicit method. Based on these reasons, the Euler explicit method is used exclusively for the subsequent simulations.

C. Flux Limiters and the Inherent Numerical Dissipation

Generally speaking, the performance of the TVD schemes, Eq. (5), depends on the limiter g^ℓ_j used, and different limiters can be applied to each distinct characteristic field to result in different TVD schemes. Several flux limiters considered in the present study are summarized as follows:

$$g^\ell_j = S \cdot \max\{0, \min(\sigma_{j+1/2}\,|\,\alpha^\ell_{j+1/2}\,|\,, S \cdot \sigma_{j-1/2}\alpha^\ell_{j-1/2})\} \quad \text{(minmod1)} \tag{6a}$$

$$g^\ell_j = \text{minmod}(\alpha^\ell_{j+1/2}, \alpha^\ell_{j-1/2}) \quad \text{(minmod2)} \tag{6b}$$

$$g^\ell_j = \frac{\alpha^\ell_{j+1/2}\alpha^\ell_{j-1/2} + |\,\alpha^\ell_{j+1/2}\alpha^\ell_{j-1/2}\,|}{\alpha^\ell_{j+1/2} + \alpha^\ell_{j-1/2}} \quad \text{(van Leer)} \tag{6c}$$

$$g^\ell_j = S \cdot \max\{0, \min(2\,|\,\alpha^\ell_{j+1/2}\,|\,, S \cdot \alpha^\ell_{j-1/2}), \min(\,|\,\alpha^\ell_{j+1/2}\,|\,, 2S \cdot \alpha^\ell_{j-1/2})\} \quad \text{(superbee)} \tag{6d}$$

where $S = \text{sgn}(\alpha^\ell_{j+1/2})$. Equation (6a) is a variant of the original minmod limiter Eq. (6b), and they are referred to as minmod1 and minmod2 in the context. Equation (6c) is known as van Leer's limiter,[24] whereas Eq. (6d), recognized as the "superbee" limiter, was proposed by Roe.[18]

Sweby[21] made a thorough investigation on various flux limiters and quantified the inherent dissipation contained in each scheme using a diagram (reproduced here as Fig. 1). As demonstrated by Sweby in Fig. 1, minmod and superbee limiters correspond to the most and least dissipative conditions, whereas van Leer's limiter is a smooth curve lying in between. In other words, limiters (6c) and (6d) contain smaller amounts of dissipation and tend to generate more compressive results than the minmod limiters. The TVD schemes and their constituent limiters that will be used for subsequent studies are listed in Table 1. It will be shown that different TVD schemes may exhibit different characteristics in the compressible mixing flow calculations, leading to discrepancies in results particularly for supersonic convective Mach number flows.

D. Initial and Boundary Conditions

The initial mean flow properties of the mixing layer are summarized as follows:

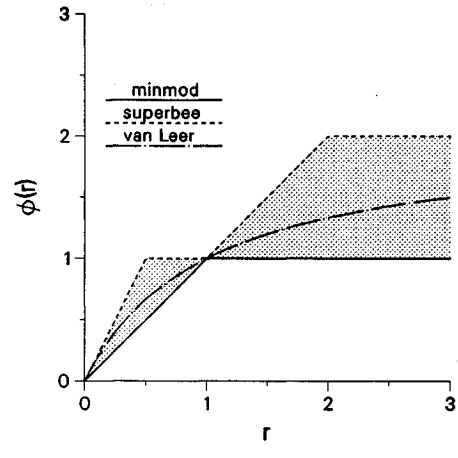

Fig. 1 Second-order TVD region and minmod, superbee, and van Leer limiters.[21]

Table 1 Summary of TVD schemes and their constituent flux limiters

TVD schemes	Nonlinear eigenfields $\lambda = u \pm c$	Linear degenerate eigenfields $\lambda = u, u$
TVDMM1	minmod1	minmod1
TVDMM2	minmod2	minmod2
TVDSB	van Leer	superbee
TVDVL	van Leer	van Leer

$$\bar{u} = M_c \tanh(y), \quad \bar{v} = 0, \quad \bar{p} = 1/\gamma M_c^2, \quad \bar{\rho} = 1 \tag{7}$$

where M_c is the convective Mach number and other variables have been defined previously. In the present study, the initial perturbations are applied only to the v velocity component in the form:

$$v' = A_1\phi_1(y)\cos(\alpha x + \theta) + A_{1/2}\phi_{1/2}(y)\cos(1/2\alpha x) \tag{8}$$

where v' is the initial perturbations superimposed on the mean flow to trigger the flow instability; $\phi_1(y)$ and $\phi_{1/2}(y)$ are the normalized eigenfunctions of the fundamental and subharmonic instability wave modes obtained from linear anlaysis; A_1 and $A_{1/2}$ represent the amplitudes of the perturbations; and θ is the phase shift between the fundamental and subharmonic modes. The present studies adopt a set of perturbation eigenfunctions from the incompressible analysis given by Michalke.[25] Although the wavenumber α of the most unstable mode, therefore the corresponding eigenfunction distributions, vary with freestream Mach number, the present compressible flow study still uses the incompressible perturbations. This strategy has already been accepted in many numerical simulations elsewhere.[15,16]

Both upper and lower boundaries of the computational domain are solid walls along which flow tangency (nonpermeable) condition is applied. The streamwise x extent of the computational domain is chosen to accommodate both fundamental and first subharmonic modes of the instability wave to assure that vortex roll-up and pairing, if they occur, will be contained in the computational domain. Periodic boundary conditions are imposed on the inflow and outflow boundaries. For the present simulations, the computational domain covers a range of $0 < x < 2\pi/\alpha$ and $-\pi/\alpha < y < \pi/\alpha$.

III. Results and Discussions

A. Grid-Independence Study

This study is devoted to the investigation of grid resolution effects in direct numerical simulations. The solution is evaluated specifically by its capability in resolving the time evolution of the large-scale vortical structures. Because the present studies are two-dimensional and neglect viscous effects, the capture of the small-scale turbulence[26] can not be assessed properly within the scope of the present study. Emphasis is, therefore, placed on the resolution of large-scale motion such as the roll-up of the shear layer and the coalescence of vortices.

A Cartesian grid system is used for the present study. The solution resolution is examined on four sets of grids, namely, 64×64, 128×128, 150×150, and 200×200 using TVDMM1 scheme. A transonic mixing flow ($M_c = 0.75$) is chosen for the present grid independence study. The reason for such a choice is because the transonic shear flow development involves simultaneously many features such as vortex roll-up, nutation, and pairing in addition to the occurrence of eddy shocklets, hence providing a good overall test for the numerical scheme. The forcing amplitudes of the fundamental and subharmonic perturbations are both set to be 1% of the mean flow velocity, with a 90-deg phase difference with each other ($A_1 = A_{1/2} = 0.01$ and $\theta = \pi/2$).

The evolution of the temporally growing shear layer can generally be quantified by the momentum thickness growth rate, which is defined by:

$$\theta = \int_{y1}^{y2} |\bar{u}(t)||1 - \bar{u}(t)|\, dy \tag{9}$$

where $\bar{u}$ is the streamwise mean velocity component. The overbar "$\bar{\ }$" denotes ensemble (Favre) average over points located on a horizontal line of the computational domain.

Figure 2 illustrates the temporal development of momentum thickness (normalized by the initial values) calculated on the four grids. In the initial stage of the evolution, the momentum thickness grows very slowly, and after $t \approx 40$ it begins to increase remarkably and reaches a maximum growth rate, signifying the roll-up of the shear layer. Momentum thickness is seen to attain a local maximum value around $t = 90$, where vortex pairing similar to that of the incompressible or low subsonic flows occurs. The subsequent evolution beyond the pairing stage is characterized by a nutation of the large coherent structures, which is illustrated in Fig. 2 by consecutive oscillations in the momentum thickness history. In Fig. 2 it can be seen that the results obtained using a 64×64 grid deviate considerably from the others and fail to capture a local maximum at the correct pairing instant when compared to those obtained by finer grids. The results given by 150×150 and 200×200 grids agree well up to the completion of the subharmonic pairing, but from this moment onward they start to depart from each other in both magnitude and phase. This is conjectured to be caused by the different amount of numerical dissipation and dispersion contained on different grids, which becomes increasingly dominant as the number of iterations accumulates.

The mean and fluctuation flowfield interaction can be examined using Favre-averaged data. The Reynolds stress distributions at $t = 98$, when vortex pairing occurs, are shown in Fig. 3. The Reynolds stresses given by the three finer grids change sign across the shear layer, indicating that reverse energy transport takes place between the mean flow and the fluctuating field. This important phenomenon has already been found in experiments when vortex pairing occurs.[4,27,28] Substantial differences are found in Fig. 3 around the three peak values, with the largest discrepancy occurring in the middle region inside the vortex core where the energy is fed from the fluctuation field back into the mean flow to suppress the shear-layer growth. This mismatch in results reveals an important characteristic of the numerical dissipation effect on the mixing flow development, namely, dissipation tends to draw energy from the mean flow and counteracts the reverse feedback of turbulent energy back to the mean shear stream. Hence, the finer or less dissipative grid (200×200) has lower

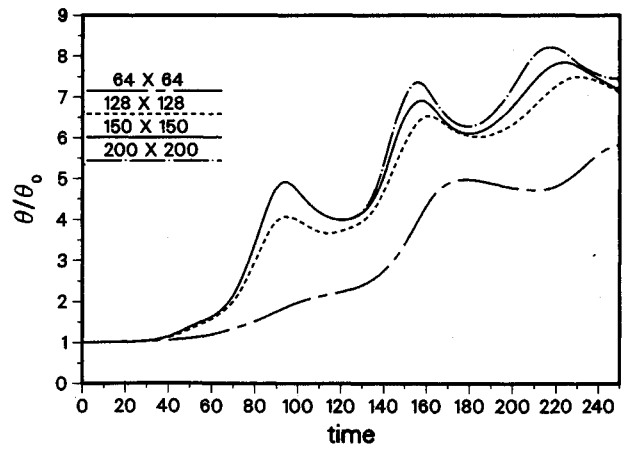

Fig. 2 A comparison of normalized momentum thickness growth histories calculated on different grids ($M_c = 0.75$).

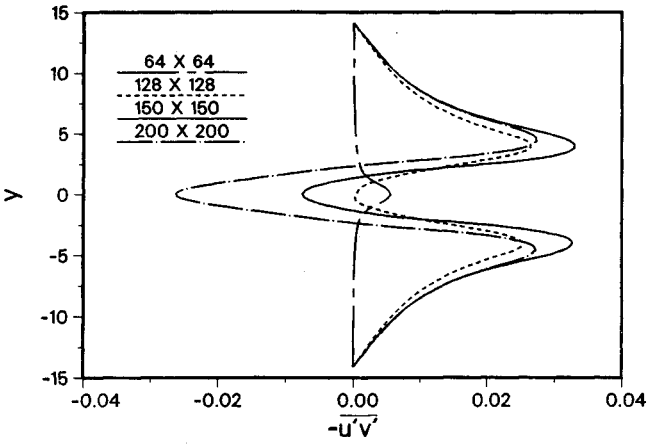

Fig. 3 A comparison of Reynolds stresses calculated on different grids (M_c = 0.75).

positive but higher negative peak values in comparison with those obtained using the coarser grid (150 × 150) (note that the Favre-averaged results on both 128 × 128 and 64 × 64 grids are not considered convergent). In other words, numerical dissipation does not always act to impede the energy transport, it is directional biased however. To intensify or to resist the energy flow depends on the direction the energy is going to flow, whether to the mean flow or to the fluctuating field. Pairing stage, therefore, provides a severe test for the numerical dissipations and Reynolds stress is very sensitive to the grid size. This sheds light on the stringent requirement of grid resolution for acquiring correct fluctuation field through the use of TVD finite volume method. Based on the overall performance evaluated, grid with 150 × 150 cells is considered to yield satisfactory results for the mixing flow computation and will be adopted as the grid for the following scheme evaluations.

B. Numerical Dissipation Effect

1. *TVD and ENO Schemes*

Recent developments of shock capturing schemes[17-21,29,30] for the computation of compressible Euler equations have been made toward generating nonoscillatory and sharply resolved solutions around shock waves and contact discontinuities. The design principle and the form of these schemes may be different in appearance, but they all originated from the Total Variation Diminishing (TVD) concept first formally proposed by Harten.[20] In order to satisfy the TVD requirements, many higher-order TVD schemes employ limiting procedures. There are two types of limiters, namely slope limiters[24,29] and flux limiters[18,21,30] that have been used in the design of TVD schemes. A slope limiter imposes constraints on the gradient of the distribution of conservative variables, while a flux limiter imposes constraints on the gradient of the flux functions.The former is often referred as MUSCL-type and the latter as non-MUSCL-type schemes, respectively. Using these limiting procedures the schemes can be designed to be second or higher order in smooth regions and to switch to first order at discontinuities and extremal points. TVD schemes by nature cannot reconcile between dissipation-free and nonoscillatory discontinuity capturing. Questions arise as to what extent this inherent local dissipation may affect the mixing flow development.

A more sophisticated discontinuity capturing algorithm termed the ENO scheme[31-33] evolved aiming at improving the order of accuracy around discontinuities and extremal points of the TVD schemes. In these newly proposed methods high order of accuracy is obtained by high-degree polynomial interpolations. However, high-degree polynomials generally do not guarantee nonoscillatory results. The compromise is to relax the TVD conditions and, instead of taking predetermined stencil points, to choose among polynomials fitting different sets of stencil points in such a way that a uniformly accurate scheme can be achieved using the least oscillatory reconstruction polynomials. The price paid for this procedure is the much elevated operational counts required because the selection of the least oscillatory stencil points is solution dependent and must be performed at each time step.

The distinction between ENO and TVD methods is that ENO schemes can retain the same spatial accuracy at extremal points where TVD schemes reduce to first order. In other words, numerical dissipation contained in the ENO scheme is intrinsically less than those of the TVD schemes. This turns out to be the major advantage for considering the ENO scheme as a good candidate for mixing flow computations. Nevertheless, ENO schemes permit oscillations up to the order of the truncation error, thus, in mixing layer problems, care should be taken to assure that the initial forcing disturbances are not swamped by the truncation and reconstruction errors, otherwise the instability will be initiated and dictated by not only the imposed disturbances, but the numerical errors as well. This shortcoming, actually, arises from the MUSCL-type reconstruction (using slope limiters) of the original data distribution. The ENO solution that is used as a benchmark to be compared with was obtained by Chen,[34] who used a uniformly second-order ENO scheme and conducted calculations on a 128 × 128 Cartesian grid. There are two alternatives of remedy to overcome the initiation problem. One is to raise the order of accuracy of the ENO scheme or to refine the grid locally near the inflection points so as to reduce the truncation errors. The other is simply to impose larger initial perturbations to outweigh the interpolation errors. The latter option was adopted by Chen. Similarly, relatively larger amplitudes of forcing are applied here, A_1 = 0.2 and $A_{1/2}$ = 0.14 for Eq. (8). With this forcing level ENO results can be used as a benchmark to assess the TVD schemes.

Numerical simulations are performed for convective Mach numbers M_c = 0.25, 0.75, and 1.5, covering subsonic, transonic, and supersonic compressible flow ranges, so that a more comprehensive study can be made to assess the characteristics of the TVD schemes when applied to mixing flow calculations.

2. *Subsonic Mixing Flow*

First, the low subsonic case M_c = 0.25 is considered, and in this test three schemes, TVDMM1, TVDSB, and ENO are used. Figure 4 illustrates the time evolution of the momentum thickness. All three schemes perform almost identically prior to the saturation of the subharmonic mode. The structures predicted by these three schemes are very similar, and TVD schemes give slightly more diffusive vortex cores due to larger dissipations in comparison with the ENO result. The Favre-

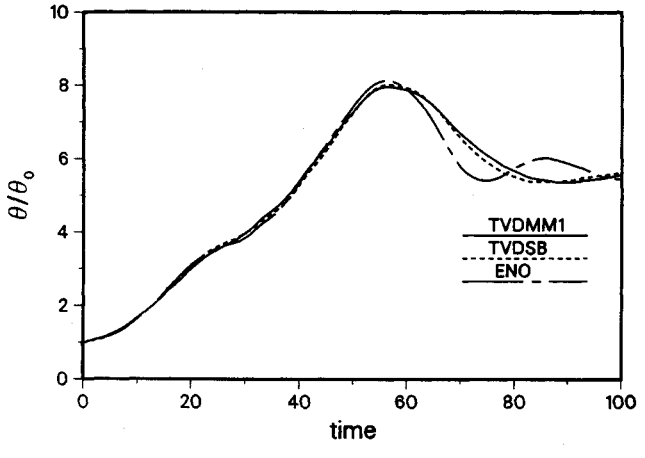

Fig. 4 A comparison of normalized momentum thickness growth histories obtained by various numerical schemes (M_c = 0.25).

averaged quantities[35] for these three schemes nearly collapse together. Because no discontinuities exist in the present low-speed compressible flowfield, the activtion of TVD limiters only takes place around the vortex core centers where solutions reach their extremal values. Generally speaking, for the low subsonic case, the performance of TVD schemes makes no substantial difference as compared to the ENO scheme.

3. Transonic Mixing Flow

The second case considers a transonic mixing flow M_c = 0.75 and four schemes, TVDMM1, TVDMM2, TVDSB, and ENO, are used. The temporal evolutions of the momentum thickness growth are demonstrated in Fig. 5. As indicated in this figure, each scheme predicts the first local maximum approximately at the same instant, however with different peak values. The maximum values obtained by TVD schemes are significantly lower than that obtained by the ENO scheme. This may be attributed to the intrinsic clipping phenomenon of TVD schemes around extremal points and discontinuities. From the pairing stage onward, the TVD and ENO results depart markedly from each other, indicating the effect of dissipation, although local, can become so dominant as to change the whole flow structure qualitatively as calculation proceeds. Figure 6 exhibits the vorticity contour lines at the instant t = 74 when the large structure reaches its maximum size due to subharmonic pairing. As shown in Fig. 6, a pair of eddy shocklets attached to the vortex cores are seen. The clean capture of these eddy shocklets can be illustrated in the streamwise pressure distribution at y = 2.5 (Fig. 7). In general, four schemes produce similar portraits of the large-scale coherent structure. Results obtained using schemes TVDMM1 and TVDMM2 are found to be more dissipative in terms of the much smoother contour lines and relatively loose structures. Scheme TVDSB, among the tested TVD variants, yields the closest results to those of the ENO scheme. This is anticipated and can be interpreted from the construction of the "superbee" limiter in which the least dissipation was used.[21] Nevertheless, as the calculation continues on, the TVDSB scheme shows reversed effect (see Fig. 5), starting around t = 120, to make the flow evolute into a unique but erroneous situation caused by the overcompression of the superbee limiter. Hence, it can be inferred that the design of the TVD limiters for high-speed mixing flow simulation is a very delicate task, either excessive or insufficient addition of dissipation could lead to significant changes in results. The overcompression characteristics of the TVDSB scheme is discussed in more detail in the subsequent supersonic mixing flow case. The vorticity contour lines generated by the ENO scheme contain small wiggles due to the fact that the ENO scheme allows for small oscillations of the truncation order. But in all, ENO scheme performs most reliably and provides the least dissipative results without creating an anomalous overcompression phenomenon.

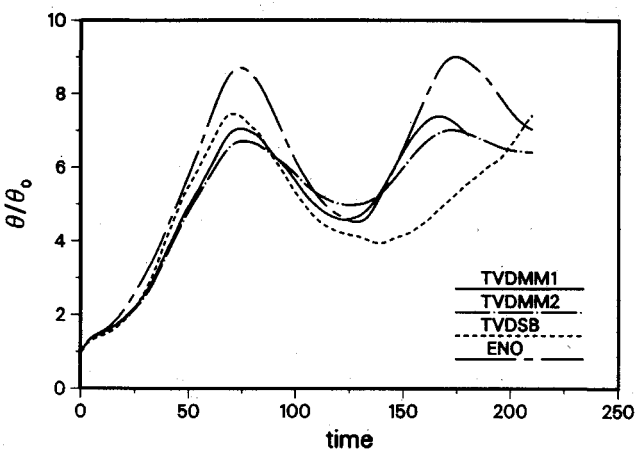

Fig. 5 A comparison of normalized momentum thickness growth histories obtained by various numerical schemes (M_c = 0.75).

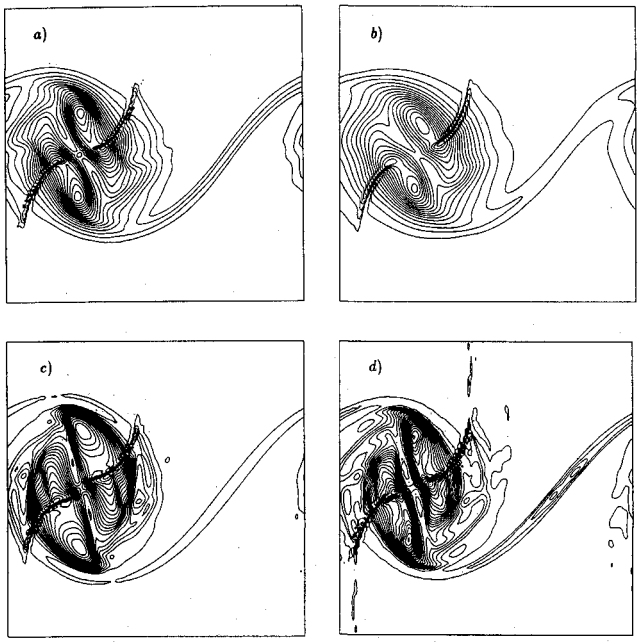

Fig. 6 Vortical structures at pairing stage predicted by various numerical schemes (M_c = 0.75, t = 74; contour lines from −0.39 to −0.01, increment 0.02). a) TVDMM1, b) TVDMM2, c) TVDSB, d) ENO.

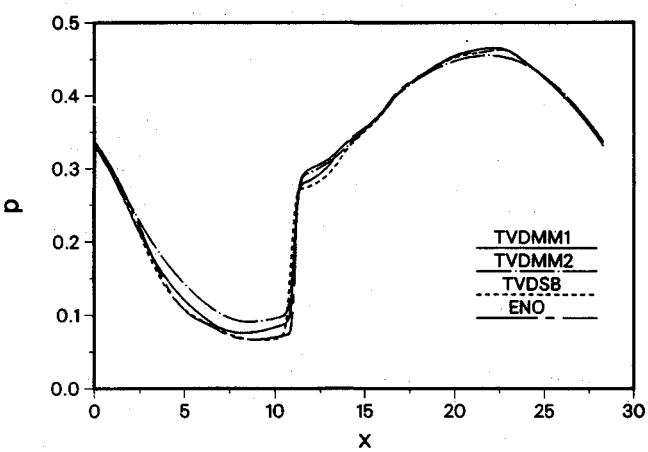

Fig. 7 A comparison of streamwise pressure distributions predicted by various schemes (M_c = 0.75, t = 74, and y = 2.5).

Figure 8 presents the instantaneous Reynolds stress distribution at the vortex pairing moment t = 74. The mismatch in data arising from using different schemes becomes more prominent on this occasion. One should be careful in interpreting the Reynolds stress results because the ENO result does not serve as an envelope, as it should be if inherent dissipation is the mechanism characterizing these high resolution schemes, to the curves presented. Referring back to Fig. 5 (the momentum thickness growth history) and after a close-up examination of the curves it can be found that at time t = 74, the TVDMM2 and ENO results reach almost right on their local maxima while the others, TVDMM1 and TVDSB, have already cleared the highest peak values and are on the way of declination. Physically, fore and aft of the local maximum the solutions are quite different in terms of the energy transport direction associated with the mean and fluctuation (turbulent) flowfields. Prior to the local maximum, the fluctuation flowfield keeps on extracting energy from the

mean shear stream to make the momentum thickness grow, but after the local maximum, the fluctuation flowfield gets saturated and starts to feed energy back to the mean flow to result in the decrease of the momentum thickness. Therefore, in Fig. 8, TVDMM2 and ENO results produce positive Reynolds stresses across the entire shear layer and TVDMM1 and TVDSB display over the central region of the shear layer some negative-valued Reynolds stress distributions. This indicates that TVD and ENO schemes basically produce the same physical results discovered experimentally, which increase their potential to be accepted as analysis tools for the mixing flow investigation.

Based on the comparisons made so far for subsonic and transonic mixing layers, TVDSB seems to be the best TVD scheme, and a TVDMM2 scheme gives the most damped solution owing to its comparatively large dissipation introduced by the limiter.

4. Supersonic Mixing Flow

The ultimate goal of the present work is to investigate supersonic mixing layers, and a case of $M_c = 1.5$ is considered in this temporal study. The momentum thickness developments are depicted in Fig. 9. For this supersonic convective Mach number, no obvious local maximum or vortex pairing can be identified in the time evolution history of the momentum thickness. All the momentum thickness curves increase with time, and greater discrepancies are found among schemes. As indicated in Fig. 9, TVD schemes consistently generate more dissipative results, which are bounded by the ENO envelope, and TVDSB scheme yields an entirely different time evolution profile. The present results fail to support the previous conclusion made for subsonic and transonic case that TVDSB is the best TVD scheme under consideration. It seems that the superbee limiter does not perform in the proper manner as predicted by Sweby[21] when used for computing supersonic mixing problems. In order to isolate the effect of the superbee limiter, another TVD scheme using exclusively the van Leer's limiters, hereafter abbreviated TVDVL, is also employed. The evolution history obtained by this scheme is also plotted in Fig. 9. It can be found that TVDVL performs in a way much closer to TVDMM1 and ENO than to TVDSB. Consequently, it may be inferred that the superbee limiter is too compressive to be used in calculating supersonic mixing layers.

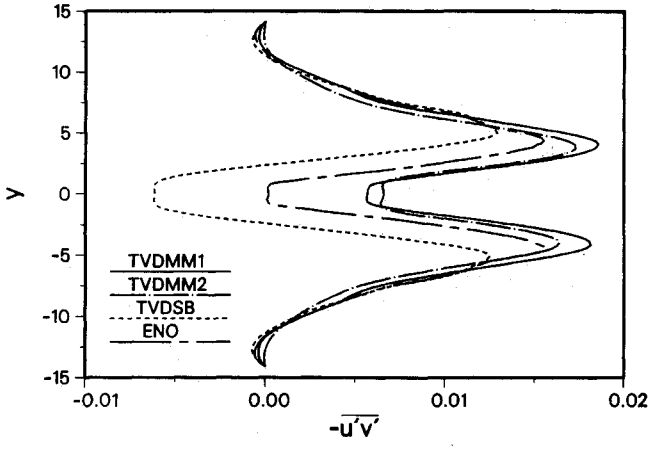

Fig. 8 A comparison of Reynolds stresses obtained by various numerical schemes ($M_c = 0.75$).

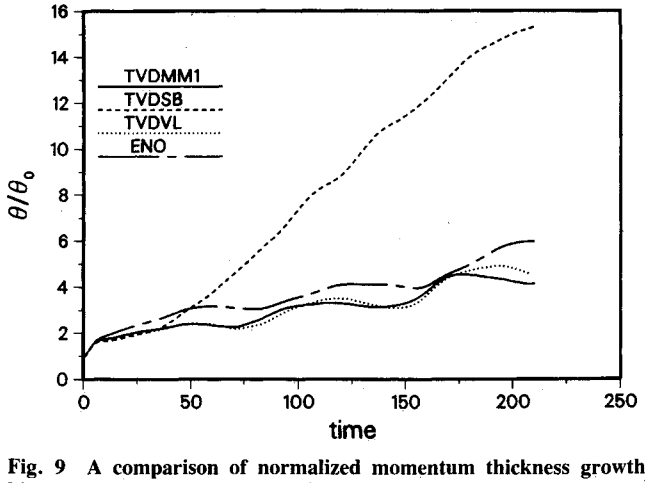

Fig. 9 A comparison of normalized momentum thickness growth histories obtained by various numerical schemes ($M_c = 1.5$).

The constant vorticity lines, shown in Fig. 10, for each scheme at the time of $t = 198$ display a set of very thin and flattened vortical structures. Moreover, the structure obtained by using the TVDSB scheme shows a completely different outlook. This, again, is caused by the superbee limiter, which overly compresses the shocklets. The qualitative difference between TVDSB and TVDVL results at this supersonic convective Mach number clearly indicates that the design of TVD limiters is a matter of great delicacy: dissipation introduced by a limiting procedure should be kept as minimal as possible, but a nonsmooth minimization such as the superbee construction (see Fig. 1) should be avoided, because it may result in nonphysical overcompression, particularly for high convective Mach number flows.

The corresponding Mach number contour plot is displayed in Fig. 11. It is found that, as the convective Mach number becomes high supersonic, the roll-up of the shear layer will generate much stronger and more far-reaching eddy shocklets. In such a high Mach number flow, shock waves become oblique and are no longer normal to the walls. The wall-reflected shock waves may interact with the shear layers to result in the so-called supersonic feedback mechanism.[12] This supersonic feedback loop can be illustrated using Mach number contour plots (Fig. 11). The region with dotted lines in the central portion of the shear layer establishes a "subsonic corridor" in which upstream communication can be allowed. In incompressible and subsonic mixing flows, this upstream feedback mechanism is the key factor for vortex pairing and

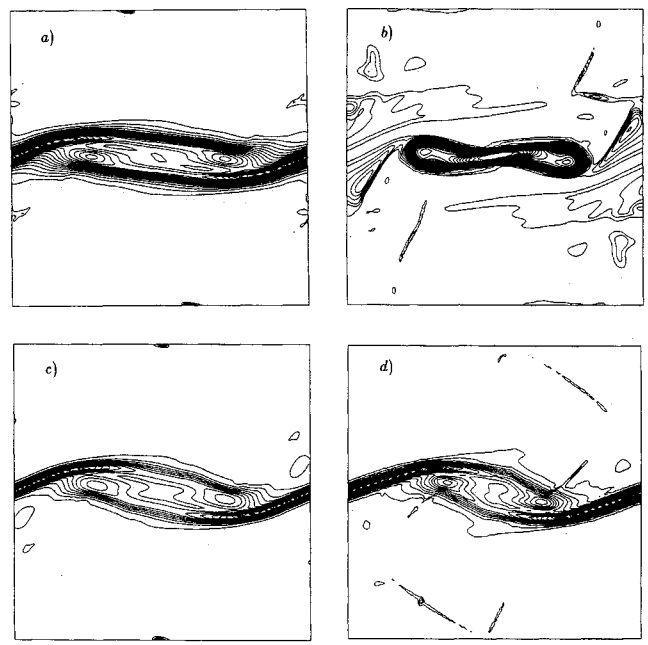

Fig. 10 Vortical structures predicted by various numerical schemes ($M_c = 1.5$, $t = 198$; contour lines from -1.06 to -0.02, increment 0.04). a) TVDMM1, b) TVDSB, c) TVDVL, d) ENO.

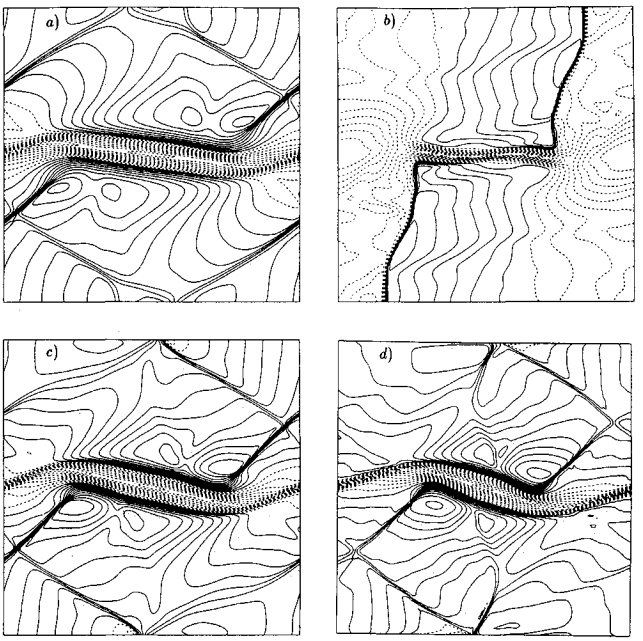

Fig. 11 Mach number contour plots predicted by various numerical schemes (M_c = 1.5, t = 198; contour lines from 0.1 to 2.1, increment 0.1). a) TVDMM1, b) TVDSB, c) TVDVL, d) ENO.

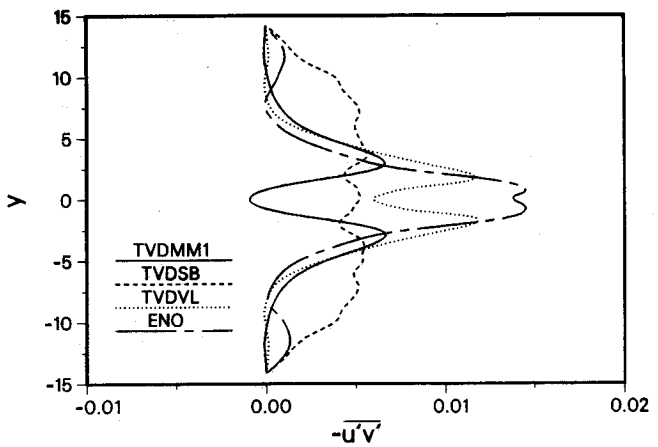

Fig. 12 A comparison of Reynolds stresses obtained by various numerical schemes (M_c = 1.5).

self-sustained oscillation to occur.[3] However, in supersonic convective Mach number flows, this feedback mechanism is largely obstructed and confined only within a narrow subsonic corridor.[6] The constraining wall plays a vital role in providing an additional route in closing up the feedback loop. Any downstream modification of the flow pattern (e.g. the roll-up of the vortical structure) will immediately alter the nearby outer attached shock or Mach wave structure and send disturbances obliquely back to the remote upstream via the confining walls. If the wall confinement is otherwise nonexistent, upstream communication can only take place within the subsonic corridor, which will become progressively inefficient as convective Mach number increases and the area of the corridor reduces.

Figure 12 illustrates the Reynolds stress obtained by using different schemes. TVDMM1 and TVDSB results show large discrepancies in comparison with the ENO result. It can be observed that the diversity in solution trends deteriorates as convective Mach number increases. This can be understood because in the M_c = 1.5 case more shock waves are present, which means the amount of dissipation caused by the clipping effect increases accordingly in the flowfield. Moreover, the overcompression of the TVDSB scheme also gets strengthened more as Mach number increases. Therefore, the solution quality is found to depend much more sensitively on the construction of the TVD schemes. A careful evaluation of the TVD scheme prior to the numerical simulation is crucial in particular for high supersonic convective Mach number flows.

IV. Conclusions

Numerical simulations of temporally developing mixing layers using high resolution schemes have been carried out to investigate the effects of grid resolution and inherent numerical dissipation on the solution quality. Flow pictures, turbulent fluctuations in addition to momentum thickness growth histories were compared during the evaluation of the TVD schemes, for which ENO results were taken as benchmark basis. A summary for the findings previously obtained is listed as follows:

1) Mixing flow computations generally require high grid density to resolve the shear-layer dynamics and to interpret the mean and fluctuation flowfield interactions. Turbulent fluctuation field is comparatively much harder to be accurately resolved than the mean flowfield, and in general, discrepancies would be amplified when simulations are marched beyond the first subharmonic pairing stage.

2) Reynolds stress or turbulent energy transport is extremely sensitive to the grid resolution and the inherent scheme dissipation effects. Numerical dissipation does not always act to impede energy transport, it is directional biased however. To intensify or to resist the energy flow depends on the energy transport direction, whether to the mean flow or to the fluctuating field.

3) Among the schemes considered, the performance of TVDMM1 and TVDVL comply more consistently with the ENO results for a wide range of convective Mach numbers, while TVDSB, being the best TVD scheme for subsonic and low transonic Mach number flows, suffers from overcompression, which may lead to nonphysical solution at high supersonic convective Mach numbers.

4) For transonic mixing layers, eddy shocklets either do not reach the wall or attach to the wall with a normal angle. However, reflective oblique shock and Mach waves occur at supersonic convective Mach number flow and form a special upstream feedback route to result in a new instability mechanism. Any downstream modification of the mixing layer would immediately affect the nearby outer shock structure and reflect disturbances back to the upstream by satisfying the confining wall boundary condition. Aside from the embedded subsonic corridor an additional route of feedback loop is formed, which makes the confined mixing layers more unstable than the free ones.

5) Generally speaking, TVD schemes provide a very clean capture of the shocks appearing in the compressible mixing flows. The inherent dissipation contained in the scheme is sensitive to the design of the limiters. Dissipation introduced by a limiting procedure should be kept as minimal as possible, but a nonsmooth minimization should be avoided, because it may result in nonphysical overcompression, particularly for high convective Mach number flows.

Acknowledgments

This work is partially supported by National Science Council, ROC, under Contract NSC 79-0401-E-006-44. The authors would like to thank C. M. Ho of the University of Southern California, and F. B. Hsiao of our Institute for many fruitful discussions.

References

[1]Brown, G. L., and Roshko, A., "On Density Effects and Large Structure in Turbulent Mixing Layers," *Journal of Fluid Mechanics*, Vol. 64, Pt. 4, July 1974, pp. 775–816.

[2]Winant, C. D., and Browand, F. K., "Vortex Pairing, the Mech-

anism of Turbulent Mixing Layer Growth at Moderate Reynolds Number," *Journal of Fluid Mechanics*, Vol. 63, Pt. 2, April 1974, pp. 237–255.

[3]Ho, C. M., and Huerre, P., "Perturbed Free Shear Layers," *Annual Review of Fluid Mechanics*, Vol. 16, 1984, pp. 365–424.

[4]Ho, C. M., and Huang, L. S., "Subharmonics and Vortex Merging in Mixing Layers," *Journal of Fluid Mechanics*, Vol. 119, June 1982, pp. 443–473.

[5]Chinzei, N., Masuya, G., Komuro, T., Murakami, A., and Kudou, K., "Spreading of Two-Stream Supersonic Turbulent Mixing Layers," *Physics of Fluids*, Vol. 29, No. 5, 1986, 1345–1347.

[6]Papamoschou, D., and Roshko, A., "The Compressible Turbulent Shear Layer: an Experimental Study," *Journal of Fluid Mechanics*, Vol. 197, Dec. 1988, pp. 453–477.

[7]Bogdanoff, D. W., "Compressibility Effects in Turbulent Shear Layers," *AIAA Journal*, Vol. 21, No. 6, 1983, pp. 926–927.

[8]Blumen, W., Drazin, D. G., and Billing, D. F., "Shear Layer Instability of an Inviscid Compressible Fluid. Part 2.," *Journal of Fluid Mechanics*, Vol. 71, Pt. 2, Sept. 1975, pp. 305–316.

[9]Ragab, S. A., and Wu, J. L., "Linear Instabilities in Two-Dimensional Compressible Mixing Layers," *Physics of Fluids A*, Vol. 1, No. 6, 1989, pp. 957–966.

[10]Tam, C. K. W., and Hu, F. Q., "The Instability and Acoustic Wave Modes of Supersonic Mixing Layers Inside a Retangular Channel," *Journal of Fluid Mechanics*, Vol. 203, June 1989, pp. 51–76.

[11]Sandham, N. D., and Reynolds, W. C., "Compressible Mixing Layer: Linear Theory and Direct Simulation," *AIAA Journal*, Vol. 28, No. 4, 1990, pp. 618–624.

[12]Zhuang, M., Dimotakis, P. E., and Kubota, T., "The Effect of Walls on a Spatially Growing Supersonic Shear Layer," *Physics of Fluids A*, Vol. 2, No. 4, 1990, pp. 599–604.

[13]Jou, W.-H., and Riley, J. J., "Progress in Direct Numerical Simulations of Turbulent Reacting Flows," *AIAA Journal*, Vol. 27, No. 11, 1989, pp. 1543–1556.

[14]Guirguis, R. H., Grinstein, F. F., Young, T. R., Oran, E. S., Kailasanath, K., and Boris, J. P., "Mixing Enhancement in Supersonic Shear Layers," AIAA 25th Aerospace Sciences Meeting, AIAA Paper 87-0373, Reno, NV, Jan. 1987.

[15]Lele, S. K., "Direct Numerical Simulation of Compressible Free Shear Flows," AIAA Paper 89-0374, Jan. 1989.

[16]Soetrisno, M., Eberhardt, S., Riley, J. J., and McMurtry, P., "A Study of Inviscid, Supersonic Mixing Layers Using a Second-Order Total Variational Diminishing Scheme," *AIAA Journal*, Vol. 27, No. 12, 1989, pp. 1770–1778.

[17]Colella, P., and Woodward, P. R., "The Piecewise Parabolic Method (PPM) for Gas-Dynamical Simulations," *Journal of Computational Physics*, Vol. 54, 1984, pp. 174–201.

[18]Roe, P. L., "Some Contributions to the Modelling of Discontinuous Flows," *Lectures in Applied Mathematics*, Vol. 22, Pt. 2, American Mathematical Society, Providence, RI, 1985, pp. 163–194.

[19]Yee, H. C., "Construction of Explicit and Implicit Symmetric TVD Schemes and Their Applications," *Journal of Computational Physics*, Vol. 68, 1987, pp. 151–179.

[20]Harten, A., "High Resolution Schemes for Hyperbolic Conservation Laws," *Journal of Computational Physics*, Vol. 49, 1983, pp. 357–393.

[21]Sweby, P. K., "High Resolution Schemes Using Flux Limiters for Hyperbolic Conservation Laws," *SIAM Journal of Numerical Analysis*, Vol. 21, 1984, pp. 995–1011.

[22]Roe, P. L., "Approximate Riemann Solvers, Parameter Vectors, and Difference Schemes," *Journal of Computational Physics*, Vol. 43, 1981, pp. 357–372.

[23]Venkatakrishnan, V., and Jameson, A., "Computational of Unsteady Transonic Flows by the Solution of Euler Equations," *AIAA Journal*, Vol. 26, No. 8, 1988, pp. 974–981.

[24]van Leer, B., "Towards the Ultimate Conservative Difference Scheme. II. Monotonicty and Conservation Combined in a Second-order Scheme," *Journal of Computational Physics*, Vol. 14, 1974, pp. 361–370.

[25]Michalke, A., "On the Inviscid Instability of the Hyperbolic Tangent Velocity Profile," *Journal of Fluid Mechanics*, Vol. 19, Pt. 4, Aug. 1964, pp. 543–556.

[26]Rogallo, R. S., and Moin, P., "Numerical Simulation of Turbulent Flows," *Annual Review of Fluid Mechanics*, Vol. 16, 1984, pp. 99–137.

[27]Metcalf, R. W., Orszag, S. A., Brachet, M. E., Menon, S., and Riley, J. J., "Secondary Instability of a Temporally Growing Mixing layer. *Journal of Fluid Mechanics*, Vol. 184, Nov. 1987, pp. 207–243.

[28]Oster, D., and Wygnanski, I., "The Forced Mixing Layer Between Parallel Streams," *Journal of Fluid Mechanics*, Vol. 123, Oct. 1982, pp. 91–130.

[29]van Leer, B., "Towards the Ultimate Conservative Difference Scheme. V. A Second-Order Sequel to Godunov's Method," *Journal of Computational Physics*, Vol. 32, 1979, pp. 101–136.

[30]Boris, J. P., and Book, D. L., "Flux-Corrected Transport. 1. SHASTA, a Fluid Transport Algorithm That Works," *Journal of Computational Physics*, Vol. 11, 1973, pp. 38–69.

[31]Harten, A., "On High-Order Accurate Interpolation for Non-Oscillatory Shock-Capturing Schemes," *The IMA Volumes in Mathematics and its Applications*, Vol. 2, Springer-Verlag, New York, 1986, pp. 71–106.

[32]Harten, A., Engquist, B., Osher, S., and Chakravarthy, S. R., "Some Results on Uniformly High-Order Accurate Essentially Non-oscillatory Scheme," *Journal of Applied Numerical Mathematics*, Vol. 2, 1986, pp. 347–377.

[33]Harten, A., Engquist, B., Osher, S., and Chakravarthy, S. R., "Uniformly High Order Accurate Essentially Non-Oscillatory Scheme III," *Journal of Computational Physics*, Vol. 71, 1987, pp. 231–303.

[34]Chen, S. K., "Numerical Investigation of Compressible Mixing Flow Using Essentially Non-Oscillatory Scheme," M.S. Thesis, Inst. of Aeronautics and Astronautics, National Cheng Kung Univ., Tainan, Taiwan, ROC, June 1990.

[35]Wu, K. C., "Numerical Investigation of Confined Supersonic Mixing Flow," Ph.D. Thesis, Institute of Aeronautics and Astronautics, National Cheng Kung University, Tainan, Taiwan, ROC, June 1991.